Bulletin of the Seismological Society of America, Vol. 88, No. 5, pp. 1212–1223, October 1998

Seismic-Reflection Evidence That the Hayward Fault Extends into the Lower Crust of the San Francisco Bay Area, California

by Tom Parsons

Abstract This article presents deep seismic-reflection data from an experiment across San Francisco Peninsula in 1995 using large (125 to 500 kg) explosive sources. Shot gathers show a mostly nonreflective upper crust in both the Franciscan and Salinian terranes (juxtaposed across the San Andreas fault), an onset of weak lower-crustal reflectivity beginning at about 6-sec two-way travel time (TWTT) and bright southwest-dipping reflections between 11 and 13 sec TWTT. Previous studies have shown that the Moho in this area is no deeper than 25 km (~8 to 9 sec TWTT). Three-dimensional reflection travel-time modeling of the 11 to 13 sec events from the shot gathers indicates that the bright events may be explained by reflectors 15 to 20 km into the upper mantle, northeast of the San Andreas fault. However, upper mantle reflections from these depths were not observed on marine-reflection profiles collected in San Francisco Bay, nor were they reported from a refraction profile on San Francisco Peninsula. The most consistent interpretation of these events from 2D raytracing and 3D travel-time modeling is that they are out-of-plane reflections from a high-angle (dipping ~70° to the southwest) impedance contrast in the lower crust that corresponds with the surface trace of the Hayward fault. These results suggest that the Hayward fault truncates the horizontal detachment fault suggested to be active beneath San Francisco Bay.

Introduction

Beneath about 15 to 20 km, the major strike-slip faults of the San Francisco Bay area strain aseismically (Olson and Lindh, 1985; Dewey *et al.,* 1989; Hill *et al.,* 1990; Lisowski *et al.,* 1991; Olson and Zoback, 1992). The lack of earthquake hypocenters beneath that depth has left many unresolved questions about the relationships among the steeply dipping right-lateral transform faults that make up the San Andreas fault zone in the San Francisco Bay area (Fig. 1) within the ductile regime. A variety of tectonic models for plate interactions in the Bay area suggest horizontal shear in the deep crust drives or at least accommodates the strain expressed at the surface (e.g., Furlong *et al.,* 1989; Furlong, 1993; Page and Brocher, 1993; Jones *et al.,* 1994; Brocher *et al.,* 1994; Bohannon and Parsons, 1995).

To learn more about the deep structure of the San Francisco Bay area and to test the hypothesis that a horizontal detachment fault is active beneath the Bay, the U.S. Geological Survey (USGS) collaborated with Woods Hole Oceanographic Institute, the University of California, Stanford University, Pennsylvania State University, and Lawrence Berkeley Laboratory on a seismic investigation in the fall of 1991 utilizing the marine waterway system that dissects the San Francisco Bay area (McCarthy and Hart, 1993) (Fig. 1). These studies, known as the Bay area seismic imaging experiments, or BASIX, consisted of complementary seismic reflection and refraction profiling methods. In 1995, large explosive sources were recorded on a fixed land array oriented southwest to northeast across San Francisco Peninsula, perpendicular to the surface trace of the San Andreas fault. These explosive sources were detonated to calibrate a local earthquake array, to determine the shallow velocity structure across the San Andreas and Pilarcitos faults, and to observe the deep reflective texture across the San Andreas fault. In this article, I present and interpret the deep reflection data; the velocity structure results were reported by Parsons and Zoback (1997).

Tectonic Setting and Geology of San Francisco Peninsula and Bay Region

The San Francisco Bay region lies within the surface expression of a broad (~70 to 80 km wide) plate boundary zone between the Pacific and North American plates. As a result, the region is highly deformed and faulted, and it includes major seismic hazards as evidenced by the 1989 M 7.1 Loma Prieta and 1906 M_w 7.7 (e.g., Thatcher, 1975) San Francisco earthquakes. Right-lateral shear takes place on several subparallel strike-slip faults (Fig. 1) such as the San

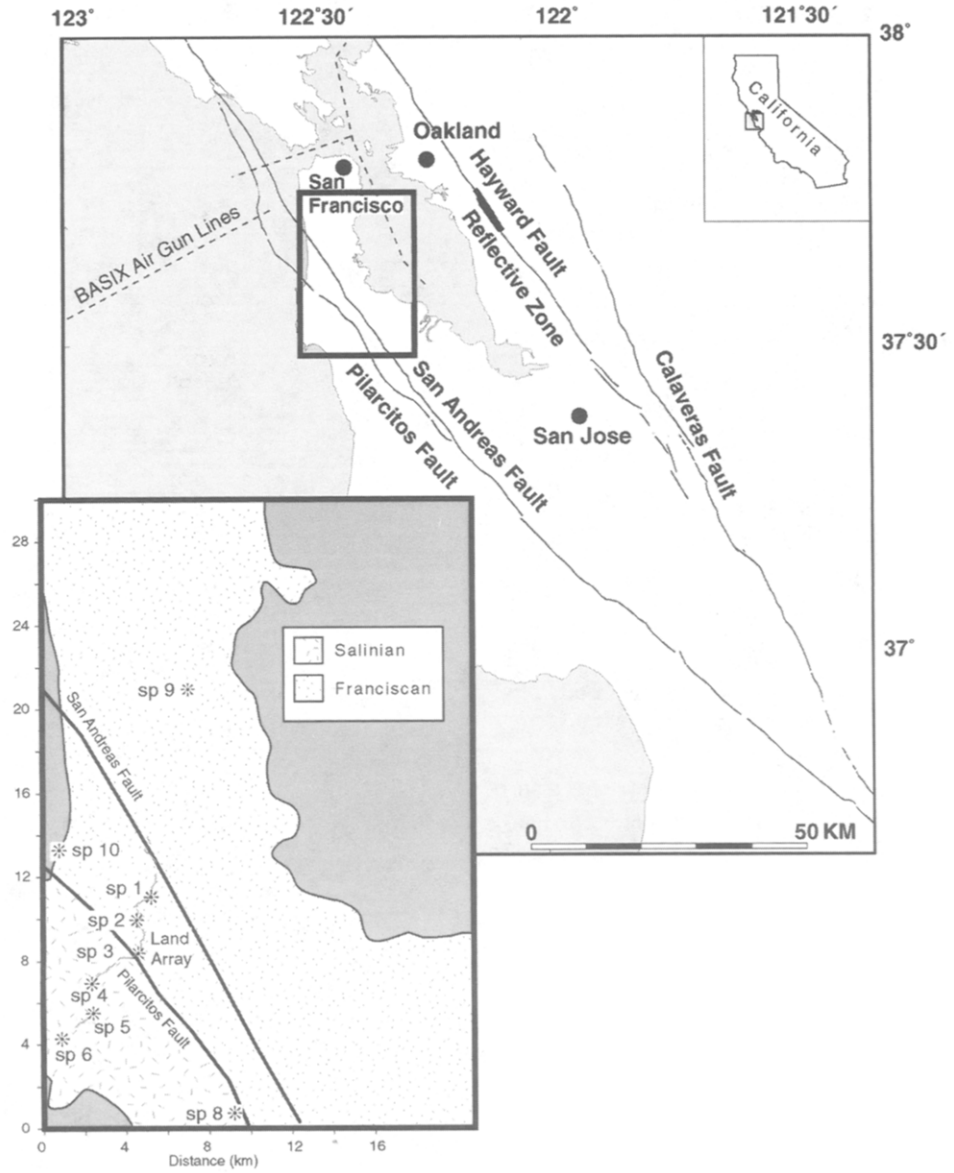

Figure 1. Tectonic setting of the San Francisco Bay region. Much of the plate boundary slip is accommodated by right-lateral motion on the San Andreas, Hayward, and Calaveras faults. The Salinian terrane is separated from the Franciscan terrane by the Pilarcitos fault on San Francisco Peninsula. The shot points (*sp*) are marked with an asterisk (*), and the receiver array is indicated by the northeast-trending gray line. A heavy black line shows the location of the reflection points beneath the surface trace of the central Hayward fault.

Andreas, Hayward, and Calaveras faults. This zone accommodates about 4 cm/yr of relative motion between the Pacific and North American plates (e.g., De Mets *et al.,* 1990; Lisowski *et al.,* 1991; Kelson *et al.,* 1992).

The San Andreas fault on San Francisco Peninsula is a relatively young feature that initiated about 1.3 to 3.3 Ma and has ~23 km of right-lateral offset (Addicott, 1969; Cummings, 1968; Taylor *et al.,* 1980; Hall, 1984, 1993; Hall *et al.,* 1996). The Pilarcitos fault west of the San Andreas acted as a "proto-San Andreas" fault prior to formation of the Peninsula segment of the San Andreas fault and may have accommodated more than 100 km of right-lateral offset (Parsons and Zoback, 1997). Faults east of San Francisco Bay (i.e., the Calaveras and Hayward) have cumulatively accommodated up to 160 to 170 km of right-lateral strain (e.g., McLaughlin *et al.,* 1996). Thus, the crust imaged southwest of the San Andreas and Pilarcitos faults on land has been offset over 100 km relative to the crust imaged beneath San Francisco Bay (above the depth extent of the vertical strike-slip faults).

Like much of coastal California, the San Francisco Bay region is underlain primarily by the late Mesozoic/early Ter-

tiary Franciscan Complex of accreted origin. This assemblage contains fragments of oceanic crust, pelagic sedimentary rocks, and continental sandstones and shales mixed together in a melange in some places and occurring as coherent units in others (e.g., Page, 1992). These rocks were emplaced during the long-term phase of oblique to head-on subduction that occurred along the California margin, and many were subsequently translated along the coast during oblique subduction and when strike-slip motion supplanted subduction during Tertiary time (e.g., Blake, 1984). In general, Cretaceous granites of the Salinian terrane are exposed west of the San Andreas Fault (e.g., Ross, 1978) (Fig. 1), though the Pilarcitos fault marks that boundary on San Francisco Peninsula.

The 1995 San Francisco Peninsula Reflection Experiment

In June of 1995, the USGS detonated 11 chemical explosions (125 to 500 kg) (Fig. 1) on San Francisco Peninsula, 9 of which generated useful data. The explosive sources were recorded on 183 Seismic Group Recorders (SGR) that were deployed along a southwest-to-northeast line across the Pilarcitos and San Andreas faults (Fig. 1). The SGRs were deployed at 50-m intervals in a fixed 9-km array that recorded seven in-line shots spaced between 1 and 5 km apart and four fan shots located between 5 and 20 km north and south of the recording profile. Because of the fairly wide shot spacing, the primary targets for the survey were the shallow velocity structure from the first arrivals (reported by Parsons and Zoback, 1997) and changes in middle and deep crustal reflectivity caused by the Pilarcitos and San Andreas faults. Table 1 shows the shot locations and every 10th receiver position. Standard reflection processing included elevation and residual statics, predictive deconvolution, and bandpass filtering (6 to 18 Hz). A 2.5-sec trailing automatic gain control (AGC) window was applied to prevent shadowing beneath the first arrivals and other prominent events.

Table 1
Locations of Explosive Sources Detonated on San Francisco Peninsula in 1995, and Locations of Every 10th Receiver Position on the Fixed Recording Spread

Shot	N Latitude	W Longitude	Elevation (m)
*1	37.59389	122.4429	342
*2	37.58404	122.45079	331
3	37.56985	122.45021	297
4	37.56501	122.46099	318
5	37.54171	122.47828	106
6	37.52051	122.50137	8
*8	37.50064	122.39841	127
*9	37.68308	122.42121	87
*10	37.6142	122.49282	0
Station (every 10th)	**N Latitude**	**W Longitude**	**Elevation (m)**
985	37.53813	122.48434	74
995	37.5405	122.47993	78
1005	37.55727	122.47437	451
1015	37.56093	122.4704	377
1025	37.56342	122.46623	319
1035	37.56726	122.46047	268
1045	37.56778	122.45513	295
1055	37.57011	122.44806	319
1065	37.57427	122.44857	317
1075	37.57803	122.44674	366
1085	37.58237	122.45034	352
1095	37.58762	122.44982	336
1105	37.5915	122.44854	273
1115	37.59336	122.44398	326
1125	37.5975	122.44187	233
1135	37.60139	122.44007	167
1145	37.61007	122.44074	123
1155	37.61305	122.44487	167
1165	37.6187	122.4439	109

*Indicates 11- to 13-sec reflections observed.

Crustal Reflectivity beneath San Francisco Peninsula

The shot gather shown in Figure 2 is representative of the vertical incidence data collected on San Francisco Peninsula. The experiment was not designed to image the shallowest crust, and the wide (~3 km) shot spacing leaves gaps in near-surface coverage. Thus, no reflection signature of either the Pilarcitos or the San Andreas fault is detected on any of the vertical incidence shot gathers. Velocity anomalies identified from refractions of controlled and earthquakes sources were noted across both structures by Parsons and Zoback (1997). The receiver spread crossed the Salinian terrane southwest of the Pilarcitos fault and the Franciscan Complex between the Pilarcitos and San Andreas faults (Fig. 1). Where imaged, these bedrock units are nearly transparent to vertical incidence energy (no coherent reflections observed) down to about 5- to 6-sec two way travel time (TWTT) (~14 to 15 km depth) over the entire source bandwidth (2 to 40 Hz).

Below about 5 to 6-sec TWTT, an onset of discontinuous middle and lower crustal reflectivity (individual crustal reflection segments are generally shorter than 1 km in length) can be seen that extends to the inferred Moho (9-sec TWTT; 27 to 28 km depth). This depth for Moho is in reasonably close agreement with models from wide-angle seismic data (Catchings and Kohler, 1996; Holbrook *et al.,* 1996) that found Moho depths between 22 and 26 km beneath the Golden Gate and near San Francisco Bay; a slightly thicker crust might be expected beneath the uplifted topography of the western San Francisco Peninsula. The reflection data do not show a discrete Moho reflection, but rather a progressive decrease of reflectivity that can be traced most clearly on the amplitude decay curve shown in Figure 2.

The onset of middle and lower crustal reflectivity at 5- to 6-sec TWTT occurs at about the same travel time as prominent events beneath San Francisco Bay observed from the 1991 BASIX experiment (~6-sec TWTT; Brocher *et al.,* 1994) and corresponds to a step in crustal velocity (6.4 to 7.3 km/sec) at ~20 km depth as modeled by Holbrook *et al.*

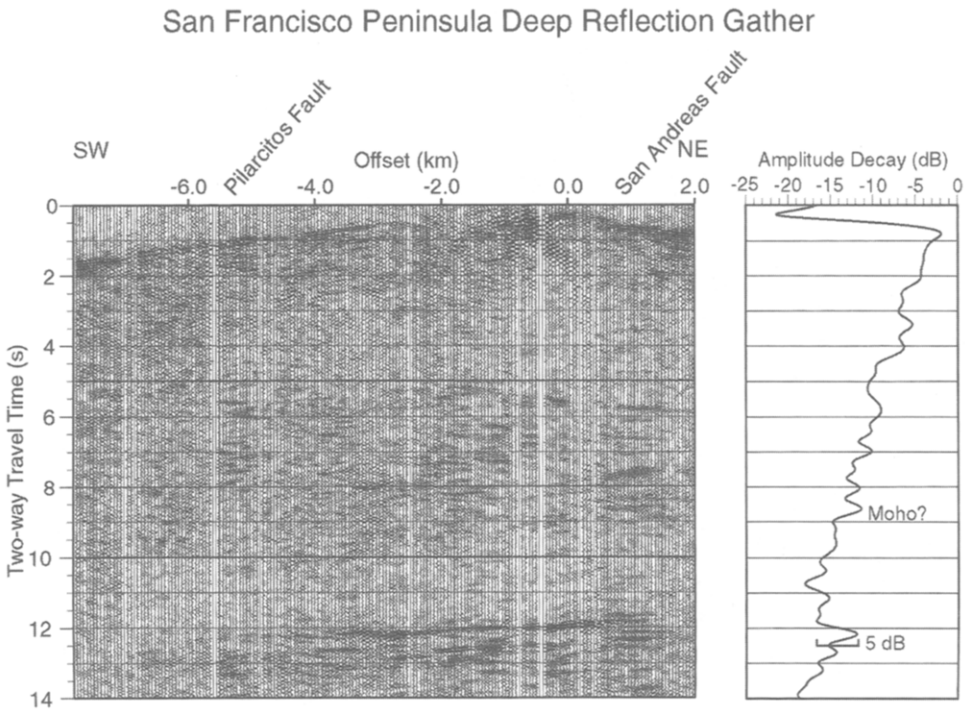

Figure 2. A representative shot gather from an explosive source recorded by 183 Seismic Group Recorders. The section shows a relatively transparent upper crust (no coherent reflections) in both the Salinian and Franciscan terranes. An onset of discontinuous middle and lower crustal reflectivity occurs at about 5- to 6-sec TWTT. No obvious changes in reflectivity are apparent across the San Andreas and Pilarcitos faults on any of the shot gathers; however, beneath San Francisco Bay, there are very bright continuous reflections (Hart *et al.,* 1995). The Moho does not generate distinct reflections and is identified by a decrease in reflectivity at ~9-sec TWTT (best seen on the amplitude decay curve). Beneath the Moho, shot gathers show southwest-dipping, high-amplitude reflections (5 dB above background) at ~11- to 13-sec TWTT. The amplitude decay curve was developed from 30 traces of the gather stacked after normal moveout correction and spherical divergence correction.

(1996). Because of the wide observation in the San Francisco Bay area of an onset of reflectivity and associated change in crustal velocity at about 20 km depth, and the choppy, discontinuous nature of the reflections, I interpret the lower crustal reflectivity beneath San Francisco Peninsula as resulting from an increase in shear fabric perhaps as a consequence of a rheologic change at ~20 km depth (e.g., Holbrook *et al.,* 1996). Lower crustal reflectivity is generally observed in terranes that have been transported long distances along strike-slip faults, such as beneath the central California margin and in Alaska, and has been attributed to lower crustal shearing during translation (Beaudoin, 1994). Shot gathers do not show any discrete lateral changes in reflectivity across the Pilarcitos and San Andreas faults in the lower crust, though the subsurface coverage extends only 3.5 km northeast of the San Andreas fault. Observations from the San Francisco Bay block show much higher amplitude lower crustal reflectivity in places (Brocher *et al.,* 1994), perhaps implying a broad-scale change across the San Andreas fault.

Late-Arriving Energy at 11 to 13 Sec

Following Moho travel times (~9-sec TWTT), a band of continuous (up to 5 km in length) bright, high-amplitude reflections appears on five of the inline and fan shot gathers at about 11- to 13-sec TWTT. The relative amplitude of the 11- to 13-sec reflections is surprisingly high (5 dB above background). For reference, the relative amplitudes reported for the Death Valley, Socorro, and Surrency bright spots range from 8.5 to 10 dB; the Death Valley and Socorro bright spots were interpreted as magma bodies (Brown *et al.,* 1987). An example of one of the 11- to 13-sec events is shown in the shot gather of Figure 2. There is a consistent directivity to the 11- to 13-sec events; they all dip to the southwest and are reflected from a horizon that must be located northeast of all the shots and the recording spread.

These 11- to 13-sec events cannot be explained by *P*-wave Moho reflections because the long travel times at crustal velocities would imply at least a 40-km-thick crust beneath San Francisco Bay, which is not consistent with interpretations of wide-angle seismic data (Page and

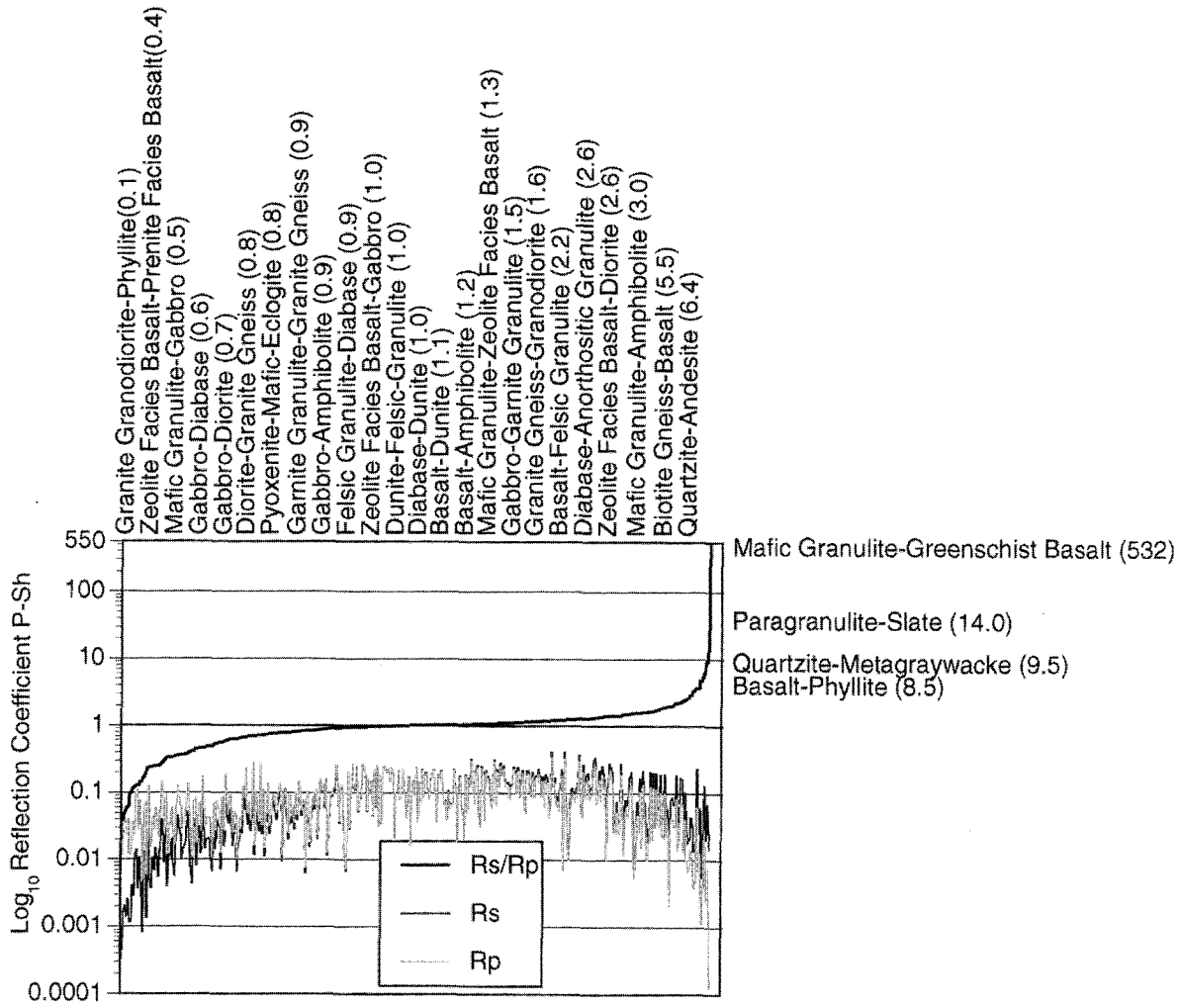

Figure 3. *P*- and *S*-wave reflection coefficients for a variety of lithologic combinations at vertical incidence. The values were calculated from the laboratory database of Christensen (1996) at a lower crustal pressure of 800 MPa; little pressure or temperature dependence on *Vp*/*Vs* ratios was noted by Christensen (1996). The upper curve shows the ratio of *S*-wave reflection coefficients to *P*-wave reflection coefficients for all the rocks in the database (812 combinations); very high values of this ratio indicate possible situations where high-amplitude *S*-wave reflections could occur without corresponding *P*-wave reflections. Example compositional contrasts and their *S*-to-*P* reflection coefficient ratios are listed along the top.

Brocher, 1993; Catchings and Kohler, 1996; Holbrook *et al.*, 1996), regional elevations, or the Bouguer gravity anomaly. This study considers four possible origins for these 11- to 13-sec TWTT reflections: (1) crustal *S*-wave reflections, (2) reflected refractions from a vertical structure, (3) upper mantle *P*-wave reflections, and (4) crustal *P*-wave reflections from steeply dipping fault zones and/or side swipe from the lower crust.

Crustal *S*-Wave Reflections

In the following discussion, I evaluate the possibility that the 11- to 13-sec reflections are *S* waves and conclude that *S* waves are an unlikely explanation, mostly because of the lack of corresponding *P*-wave reflections. If the 11- to 13-sec events are shear-wave reflections; these events would have to be direct *S*–*S* reflections because the 11- to 13-sec events are at their highest amplitude at the nearest offsets, and *P*-to-*SV* conversions are absent or very low amplitude at near offsets (e.g., Domenico and Danborn, 1987; Waters, 1987). In addition, these shear-wave reflections would have to have exceptionally high amplitudes because they were recorded on vertical geophones.

Thurber *et al.* (1996) observed high-amplitude reflections at 13-sec TWTT on three-component instruments in a similar seismic experiment conducted across the San Andreas fault in the Gabilan Range (near the intersection between the Calaveras and San Andreas faults). They concluded that the events were *S*-wave reflections based on

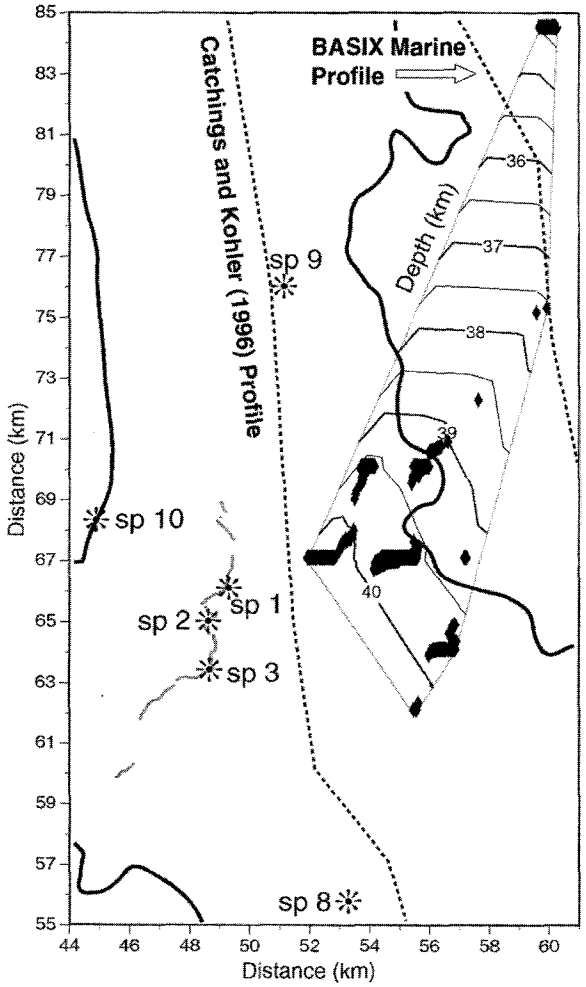

Figure 4. Results of 3D reflection travel-time modeling of the 11- to 13-sec events. Modeled reflection depth points are contoured in kilometers (as shown by the black diamonds on the contours). This model is for the lowest possible angled solution and fits a horizon between 35 and 40 km depth beneath the San Francisco Bay block. Although this model satisfies the travel-time data, deep reflection data recorded in San Francisco Bay and on the Peninsula (locations shown by dashed lines) collected above the modeled horizon show no evidence of its presence.

particle motions and higher-amplitude reflections recorded by horizontal geophones. There are, however, some unusual features of the 11- to 13-sec reflections beneath San Francisco Peninsula if they are primary *S*-wave reflections. For example, unlike the data of Thurber *et al.* (1996), strong, continuous corresponding *P*-wave reflections at ~7 to 7.5-sec TWTT were not recorded on San Francisco Peninsula (Fig. 2). This implies that if the 11- to 13-sec events are *S* waves, then they reflected from a horizon mostly transparent to *P* waves and highly reflective to *S* waves. Additionally, nearby (4 to 20 km away) three-component network stations deployed for a 3D upper crustal velocity study (Parsons and Zoback, 1997) show no strong reflection energy on the horizontal components near 11- to 13-sec TWTT.

The possibility of differing *P*- and *S*-wave reflection responses can be evaluated by investigating *P*- and *S*-wave resolution at depth and by calculating a wide range of theoretical *P*- and *S*-wave reflection coefficients. If a lower crustal reflector is too narrow an impedance gradient for *P* waves, but not for the lower-velocity (and thus with a shorter expected wavelength) *S* waves, then *S*-wave reflections could result without (or with very weak) corresponding *P*-wave reflections. Incident *S* waves would tend to have shorter wavelengths than corresponding incident *P* waves only if they had comparable frequencies. Comparison of the *Pg* and *Sg* phases on the nearby three-component network indicates that the explosive sources generated significantly lower frequency (4 to 10 Hz vs. 6 to 18 Hz at peak amplitudes) and amplitude *S* waves than the corresponding *P* waves, probably due to the greater attenuation of the *S* waves (e.g., Domenico and Danbom, 1987). Factoring in the different frequency content of source-generated *S* waves as compared with *P* waves indicates that the wavelengths of incident *P* and *S* waves are essentially the same, implying that there is no difference in their resolution, except perhaps very near to the source.

There are lithologic combinations that can generate much higher *S*-wave reflection coefficients than *P*-wave reflection coefficients. This can be shown with calculations using the database of Christensen (1996) that includes virtually every major rock classification (812 combinations) (Fig. 3). However, only two combinations meet the following basic criteria for deep crustal reflections: (1) the lithologies must be viable at lower crustal pressures and a high geothermal gradient and be roughly consistent with the observed lower crustal velocity structure, (2) the ratio of *S*- to *P*-wave reflection coefficients must exceed 2:1 for *P*-wave reflections to go unobserved (based on the relative amplitudes between observed events at 11 to 13 sec and the weakest events at 7 to 8 sec, Fig. 2), and (3) the absolute *S*-wave reflection coefficient must be equal to or greater than 0.1 [where lower crustal and Moho reflection coefficients have been calculated on highly reflective crustal data, they were found to range from 0.10 to 0.15 (e.g., Warner, 1990)]. The two combinations that meet the criteria are mafic granulite in contact with amphibolite and diabase in contact with anorthositic granulite. It is unlikely that widespread continuous contacts of these lithologies are found in the middle crust as these styles of metamorphism are characterized as patchy even at thin-section scale (e.g., Best, 1982). Additionally, the Franciscan terrane is a highly variable melange in which widespread continuous lithologic contacts are rare (e.g., Page, 1992). I thus conclude that the 11- to 13-sec reflections are *P*-wave and not crustal *S*-wave events.

Out-of-Plane *P*-Wave Reflections or Reflected Refractions

If the 11- to 13-sec reflections are not crustal *S* waves, then the problem becomes one of modeling a reflector in the

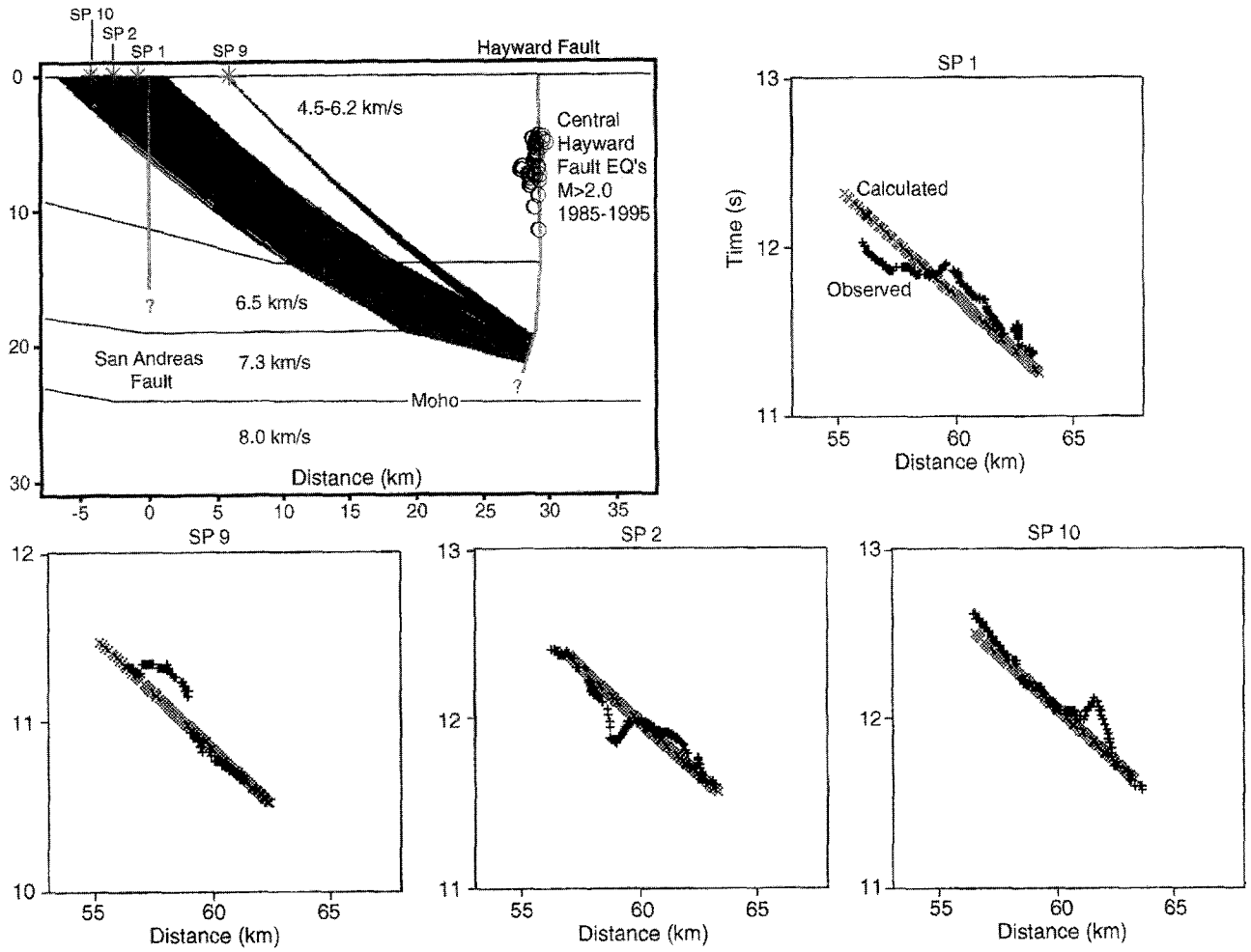

Figure 5. Two-dimensional ray paths are shown with calculated and observed travel times for four shot gathers from San Francisco Peninsula (Fig. 1) from the preferred model with a 70° dipping interface in the lower crust beneath the projection of the Hayward fault. Shallow velocity variations were not modeled, thus the advances and delays from basins and basement highs are not fit. However, the travel-time trends for all the shot gathers were matched.

crust or mantle that is most consistent with the observed *P*-wave travel times. All shot gathers with the 11- to 13-sec events show a southwest dip on the reflections (both inline and fan shots), which implies that the reflectors lie to the northeast of the sources and recording spread. There is only a small change in moveout from the inline shots to the fan shots, which indicates that the reflecting horizon dips roughly parallel to the trend of the receiver profile. If these events are interpreted as *P*-wave reflections, then the 11- to 13-sec arrival times are roughly appropriate for either reflected refractions from a vertical impedance contrast east of San Francisco Bay, reflections from a southwest-dipping upper mantle horizon (Fig. 4), or reflections from a steeply dipping (Figs. 5 and 6) deep crustal impedance contrast.

If the 11- to 13-sec events represent reflected refractions from a fault plane like those observed by Hole *et al.* (1996) from the San Andreas fault, then the apparent moveout of the events should be about 6.0 to 6.5 km/sec (Holbrook *et al.*, 1996; Parsons and Zoback, 1997). However, the observed moveout on the 11- to 13-sec events on shot gathers is closer to 10.0 km/sec (Fig. 2), indicating that the events are not reflected refractions. Thus, 3D travel-time modeling and 2D raytrace tests are conducted for a variety of dipping boundaries, assuming that the 11- to 13-sec events are *P*-wave reflections.

To model 3D reflector position from reflection travel times, the finite-difference algorithm of Vidale (1988, 1990) is extended to compute reflection travel times (Hole and Zelt, 1995) through the 3D upper crustal velocity structure of Parsons and Zoback (1997) and an extrapolation of the 2D lower crustal velocity structure of Holbrook *et al.* (1996) (Fig. 6). In the first step, first-arrival travel times are computed from a point source to the reflecting interface. This sampled travel-time field is input into the finite-difference

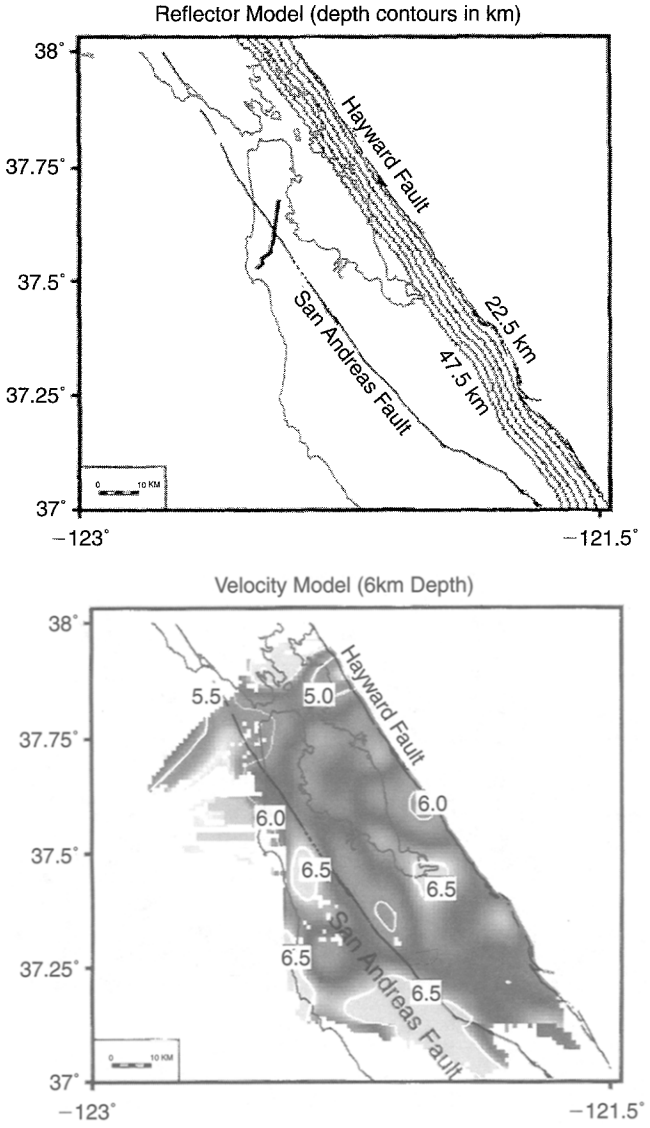

Figure 6. Three-dimensional forward model for the 11- to 13-sec reflection events. The reflector surface is vertical to 18 km depth and has a 70° dip below. Contour lines show the location of the dipping part of the horizon. An example slice through the 3D velocity model (6 km depth) is shown below.

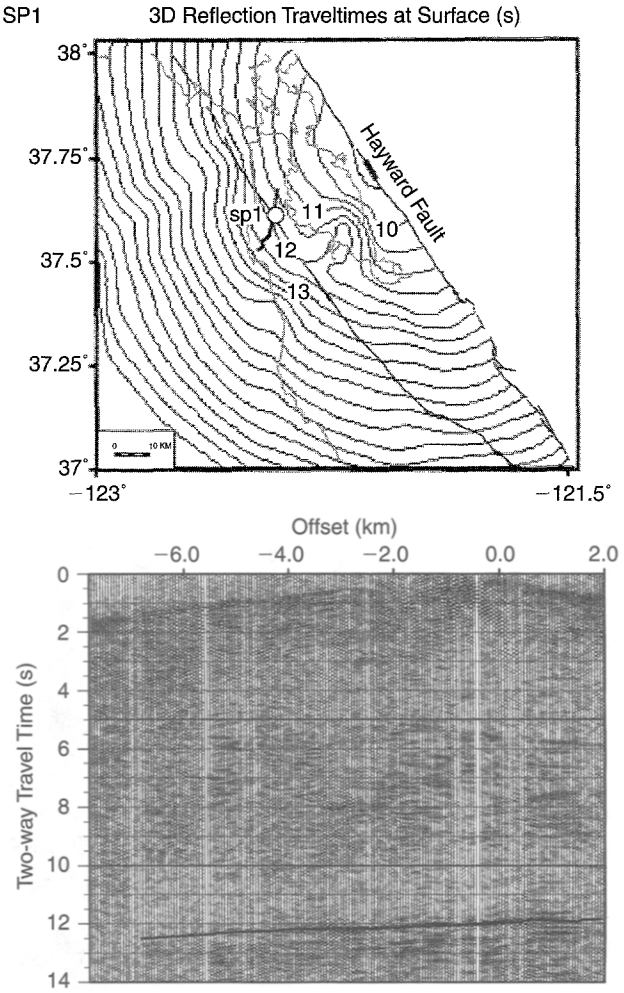

Figure 7. Reflection travel-time contours in 0.5-sec intervals are shown for inline shotpoint 1 (location shown with a circle). The reflection points are shown with a heavy black line. The shot gather is shown below with the calculated travel times indicated by a black line. Shallow velocity variations are much better fit with the 3D model.

algorithm, and travel times are computed upward from the base of the model. In this manner, the incident travel times on the reflecting interface are used as a source to propagate the reflected wave upward through the 3D model. Reflector position is determined iteratively either by inversion or by repeated forward modeling steps. Additionally, two-dimensional raytrace tests are conducted using the method of Luetgert (1992) (Fig. 5).

A 3D reflection travel-time inversion solved for a minimum-dip reflector, which corresponds to an upper mantle horizon lying between 35 and 39 km beneath San Francisco Bay (Fig. 4). The inversion results show that the reflector must dip to the southwest to satisfy the observed arrivals. The resulting root-mean-squared travel-time residual of 480 msec is larger than the estimated picking uncertainties (20 to 200 msec, depending on reflection amplitude). There are additional problems with the lowest-angled solution; deep seismic reflection data collected in San Francisco Bay did not show any reflections at post-Moho times from this area (McCarthy and Hart, 1993; Brocher *et al.*, 1994; Hart *et al.*, 1995) even though energy from the airguns employed traveled more than 100 km through the crust as turning rays (Holbrook *et al.*, 1996). Further, Catchings and Kohler (1996) did not report high-amplitude reflections from the upper mantle recorded on their refraction profile that paralleled the San Andreas fault on San Francisco Peninsula (Fig. 4).

Because of the problems associated with an upper mantle reflector beneath San Francisco Bay as the cause of the

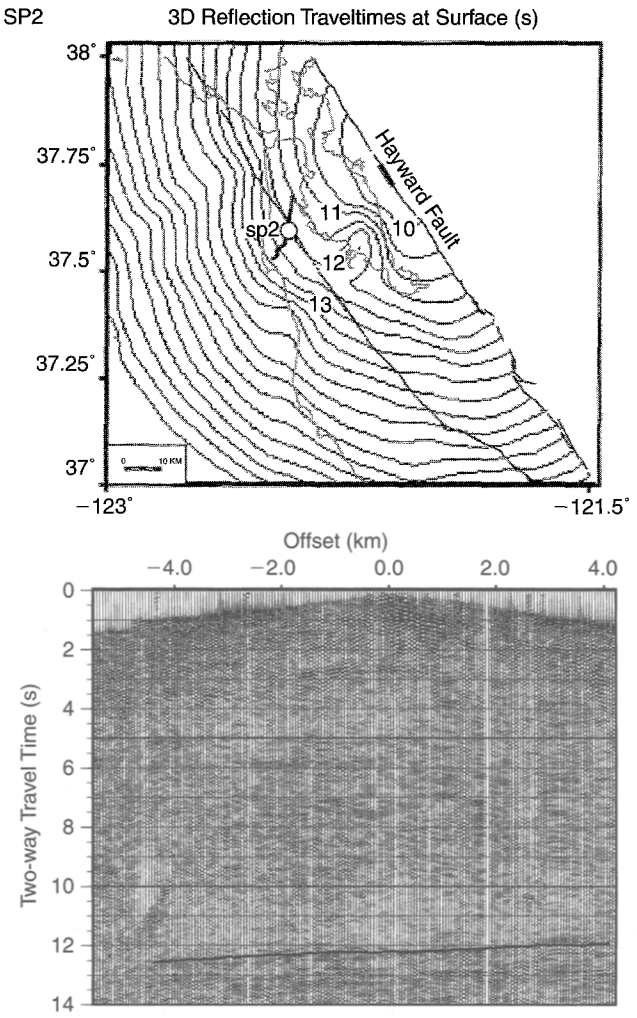

Figure 8. Reflection travel-time contours in 0.5-sec intervals are shown for inline shotpoint 2 (location shown with a circle). The reflection points are shown with a heavy black line. The shot gather is shown below with the calculated travel times indicated by a black line.

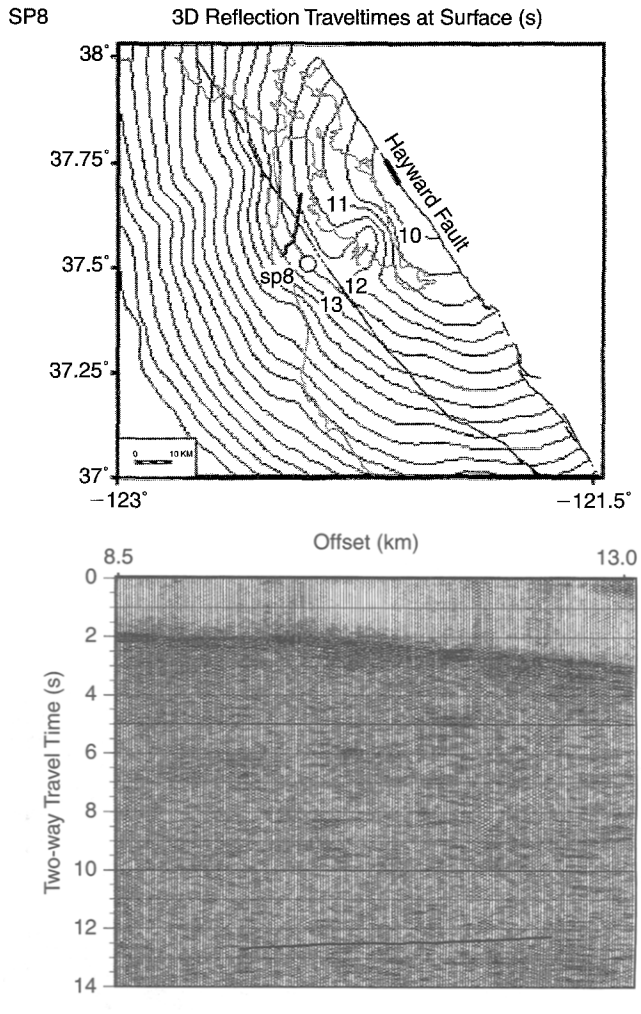

Figure 9. Reflection travel-time contours in 0.5-sec intervals are shown for fan shot 8 (location shown with a circle). The reflection points are shown with a heavy black line. The shot gather is shown below with the calculated travel times indicated by a black line.

11- to 13-sec events, I test higher-angled reflectors using a 2D raytrace method (Luetgert, 1992) and find that the travel-time trends of individual shot gathers can be satisfied by a steeply (~70°) west-dipping interface in the lower crust beneath the surface trace (and vertical projection of the fault to 18 km based on seismicity) of the Hayward fault (Fig. 5). For the 2D modeling, I assume that the velocity structure is relatively homogeneous parallel to the Hayward and San Andreas faults and project the shot positions into the plane of the 2D model of Figure 5 such that the energy from the sources takes the shortest path to the lower crustal reflector. This approach generates reasonable fits to the travel-time trends of the various shot gathers apart from near-surface velocity variations.

Because the 2D raytrace tests establish a high-angled reflector (70° dip) in the lower crust as a potential cause of the 11- to 13-sec reflections, 3D forward modeling is conducted to take advantage of small changes in reflection moveout caused by the crooked geometry of the recording spread, inline and fan geometry source locations, and knowledge of the regional 3D velocity structure to enhance the potential directivity of the events. I define a model in which the fault is vertical to a depth of 18 km and then dips at a constant 70° to the southwest along its length (Fig. 6) based on the 2D model shown in Figure 5. Utilizing the 3D upper crustal velocity model of Parsons and Zoback (1997) and applying a uniform lower crustal velocity model after Holbrook *et al.* (1996), I calculate travel times from five explosive sources to the dipping fault (Fig. 7 through 11). This model satisfies all the observed travel times and fits the arrivals well within the estimated picking errors of 20 to 200 msec (Fig. 7 through 11). Subtle variation in reflection arrival times caused by source-receiver geometry and variable ray-path velocities are closely fit by the forward model. The

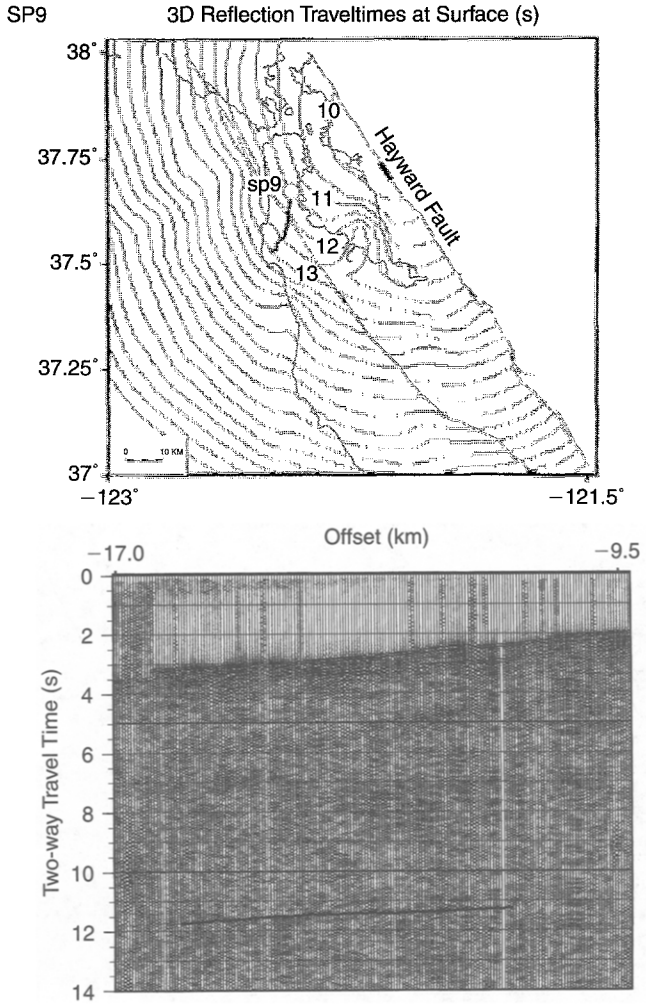

Figure 10. Reflection travel-time contours in 0.5-sec intervals are shown for inline shotpoint 9 (location shown with a circle). The reflection points are shown with a heavy black line. The shot gather is shown below with the calculated travel times indicated by a black line.

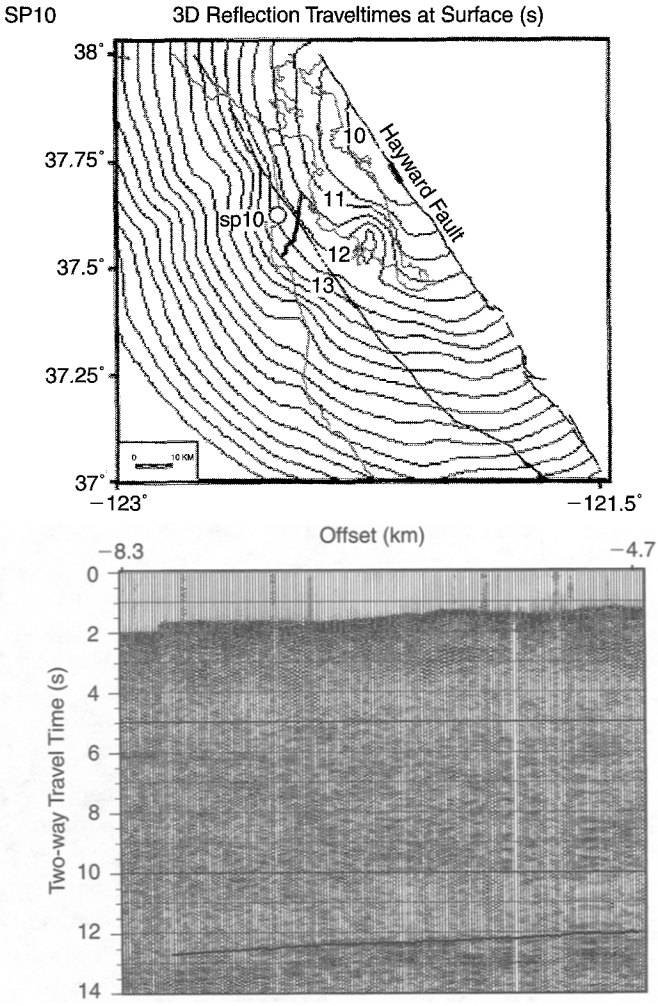

Figure 11. Reflection travel-time contours in 0.5-sec intervals are shown for fan shot 10 (location shown with a circle). The reflection points are shown with a heavy black line. The shot gather is shown below with the calculated travel times indicated by a black line.

reflection points occur along a short (~10-km-long) zone near the central Hayward fault (Figures 1 and 7 through 11).

The success of the 3D model shown in Figure 6 as compared with the lower-angled model of Figure 4, and the inherent problems with assigning the 11- to 13-sec events as crustal shear waves, leads me to conclude that the most viable reflector position is in the lower crust beneath the central Hayward fault.

Discussion

The late-arriving 11- to 13-sec reflections observed on San Francisco Peninsula show directivity and indicate that the events reflect from either a southwest-dipping horizon in the upper mantle beneath San Francisco Bay (Fig. 4) or the lower crust beneath the Hayward fault (Fig. 6). The high-angle fault reflector solution for the 11- to 13-sec events is preferred, as there are significant problems with interpreting them as shear waves or upper mantle reflections. Because of the limitations in the 3D reflection depth-point coverage (Figures 1 and 7 through 11), the data cannot confirm the presence of a 70°-dipping plane in the lower crust along the entire length of the Hayward fault, but just a small ~10-km-long patch beneath the central part of the fault.

The relatively high amplitude (~5 dB above background) of the 11- to 13-sec events signifies a strong impedance contrast in the lower crust beneath the surface trace of the Hayward fault (Figs. 5 and 6). Thus, right-lateral movement on the Hayward fault may have occurred through the whole crust and offset significantly different lithologies. The small reflective patch imaged in this study could be a fragment of anomalous velocity lower crust that was cut or rotated by motion on the Hayward fault. Alternatively, the

presence of fluids in the fault zone or localized shearing and accompanying metamorphism within the fault zone may have generated an impedance contrast (e.g., Fountain *et al.,* 1984; Wang *et al.,* 1989; Kern and Wenk, 1990; Siegesmund *et al.,* 1991). The typical width in time of the 11- to 13-sec reflections and coda is about 1 sec. However, given the uncertainties of potential near-surface reverberations and along-path scattering, it is not possible to comment on the width or possible multi-layered nature of the reflector. The very high reflection amplitudes do suggest a possible fluid-saturated zone (e.g., Brown *et al.,* 1987).

The depth to which high-angle strike-slip faults penetrate is important in resolving the possible interaction between faults beneath seismogenic depths (e.g., Furlong *et al.,* 1989) and also how much strain localizes in fault zones (e.g., Sanders, 1990). To explain the observed heat flow, crustal structure, surface compressional features, and offshore magnetic anomalies, various authors have proposed a low-angled mechanical link in the lower or middle crust that extends between the San Andreas and Hayward faults or across both (e.g., Furlong *et al.,* 1989; Furlong, 1993; Page and Brocher, 1993; Jones *et al.,* 1994; Brocher *et al.,* 1994; Bohannon and Parsons, 1995). The results of this study suggest that any such low-angle structure could be truncated by the Hayward fault and thus would favor the models of Furlong *et al.* (1989) and Furlong (1993), which have a shallow penetrating San Andreas fault, and a Hayward fault the cuts the whole crust. However, there are indications from geodetic and earthquake measurements that lower crustal slip also occurs on the San Andreas fault (e.g., King *et al.,* 1987; Sanders, 1990; Wallace *et al.,* 1991). Crustal velocity models across the San Andreas fault near the Mendocino triple junction (Henstock *et al.,* 1997) and in San Francisco Bay near the Golden Gate (Holbrook *et al.,* 1996) show evidence for upper mantle offset or lower crustal velocity anomalies associated with the fault. If high-angle strike-slip faults do tend to penetrate through the whole crust, then the implication for earthquakes occurring in the San Francisco Bay area is that strain is primarily localized to the high-angle faults throughout the whole crust, minimizing the strain occurring on low-angle structures, and that any link between the faults occurs mostly as stress transfer through the elastic crust (e.g., Stein and Lisowski, 1983).

Conclusions

The results from a deep crustal controlled-source reflection experiment reveal discontinuous reflectivity in the middle to lower crust (5- to 9-sec TWTT, ~16 to 28 km depth) that I interpret as horizontal shear fabric induced by right-lateral translation along the Pilarcitos and San Andreas fault zones. Late-arriving, post-Moho reflections that dip southwest were best fit by a high-angle (~70°) interface in the lower crust beneath the surface projection of the Hayward fault. These results suggest that the Hayward fault cuts through the entire crust and either has apparently offset significantly different rocks in the lower crust or has developed a strong impedance contrast through shearing, metamorphism, and trapping fluids.

Acknowledgments

I thank Richard Allen, Peter Barnes, Bob Bohannon, Tom Burdette, Philip Burrows, Sam Clarke, Diana Collins, Ed Criley, Lynn Dietz, Moritz Fliedner, Anne Gibbs, Niki Godfrey, Mike Hamer, John Hole, Jason Kelley, Will Kohler, Björn Lund, Richard Marsden, Andy Michael, Janice Murphy, Jean Olson, Stephanie Ross, David Rutledge, Holly Ryan, and George Thompson for their help in gathering the reflection data. Golden Gate National Recreation Area, the Crystal Springs Water District, and the San Francisco Public Utilities Commission kindly permitted access to restricted lands. This article was improved significantly because of reviews by Tom Brocher, Lind Gee, and an anonymous reviewer. This project was funded jointly by three U.S. Geological Survey programs: the Deep Continental Studies Program, the National Earthquake Hazards Reduction Program, and the Marine and Coastal Studies Program.

References

Addicott, W. A. (1969). Late Pliocene mollusks from San Francisco Peninsula, California, and their paleogeographic significance, *Proc. Calif. Academy Sci., 4th Series* **37,** 57–93.

Beaudoin, B. C. (1994). Lower-crustal deformation during terrane dispersion along strike-slip faults, *Tectonophysics* **232,** 257–266.

Best, M. G. (1982). *Igneous and Metamorphic Petrology,* W. H. Freeman and Company, New York, 630 pp.

Blake, M. C., Jr. (1984). Franciscan geology of northern California, *Field Trip Guidebook—Pacific Section, Society of Economic Paleontologists and Minerologists,* vol. 43, 254 pp.

Bohannon, R. G. and T. Parsons (1995). Tectonic implications of Post-30 Ma Pacific and North American relative plate motions, *Geol. Soc. Am. Bull.* **107,** 937–959.

Brocher, T. M., J. McCarthy, P. E. Hart, W. S. Holbrook, K. P. Furlong, T. V. McEvilly, J. A. Hole, and S. L. Klemperer (1994). Seismic evidence for a possible lower-crustal detachment beneath San Francisco Bay, California, *Science* **265,** 1436–1439.

Brown, L. D., C. E. Wille, L. Zheng, B. de Voogd, J. Mayer, T. Hearn, W. Sanford, C. Caruso, T. F. Zhu, D. Nelson, C. Potter, E. Hauser, S. Klemperer, S. Kaufman, and J. Oliver (1987). COCORP: new perspectives on the deep crust, *Geophys. J. R. Astron. Soc.* **89,** 47–54.

Catchings, R. D. and W. M. Kohler (1996). Reflected seismic waves and their effect on strong shaking during the 1989 Loma Prieta, California, earthquake, *Bull. Seism. Soc. Am.* **86,** 1401–1416.

Christensen, N. I. (1996). Poisson's ratio and crustal seismology, *J. Geophys. Res.* **101,** 3139–3156.

Cummings, J. C. (1968). The Santa Clara Formation and possible post-Pliocene slip on the San Andreas fault in central California, in *Proceedings of the Conference on Geologic Problems of the San Andreas Fault System,* W. R. Dickinson and A. Grantz (Editors), *Stanford Univ. Publ. Geol. Sci.,* **11,** 191–207.

De Mets, C., R. G. Gordon, D. F. Argus, and S. Stein (1990). Current plate motions, *Geophys. J. Int.* **101,** 425–478.

Dewey, J. W., D. P. Hill, W. L. Ellsworth, and E. R. Engdahl (1989). Earthquakes, faults, and the seismotectonic framework of the contiguous United States, in *Geophysical Framework of the Continental United States,* L. C. Pakiser, and W. D. Mooney (Editors), *Geol. Soc. Am. Mem. 172,* 541–576.

Domenico, S. N. and S. H. Danbom (1987). Shear-wave technology in petroleum exploration—past, current, and future, in *Shear-Wave Exploration,* S. H. Danbom and S. N. Dominico (Editors), Society of Exploration Geophysics. Tulsa, Oklahoma, 3–18.

Fountain, D. M., C. A. Hurich, and S. B. Smithson (1984). Seismic reflectivity of mylonite zones in the crust, *Geology* **12,** 195–198.

Furlong, K. P. (1993). Thermal-rheologic evolution of the upper mantle and the development of the San Andreas fault system, *Tectonophysics* **223,** 149–164.

Furlong, K. P., W. D. Hugo, and G. Zandt (1989). Geometry and evolution of the San Andreas fault zone in northern California, *J. Geophys. Res.* **94,** 3100–3110.

Hall, N. T. (1984). Holocene history of the San Andreas fault between Crystal Strings Reservoir and San Andreas Dam, San Mateo County, *Bull. Seism. Soc. Am.* **74,** 281–299.

Hall, N. T. (1993). Paleoseismic investigations of the San Andreas Fault on the San Francisco Peninsula, California, *U.S. Geol. Surv. Tech. Rept.,* 15 pp.

Hall, N. T., R. H. Wright, and K. B. Clahan (1996). Paleoseismic investigations of the San Andreas fault on the San Francisco Peninsula, California, *USGS-NEHRP Final Tech. Rept. 14-08-0001-G2081,* Reston, Virginia, 45 pp.

Hart, P. E., J. McCarthy, and J. R. Childs (1995). Deep seismic reflection profiling in San Francisco Bay: results from the 1995 BASIX Bay Cable project (abstract), *EOS* **76,** F398.

Henstock, T. J., A. Levander, and J. A. Hole (1997). Deformation in the lower crust of the San Andreas fault system in northern California, *Science* **278,** 650–653.

Hill, D. P., J. P. Eaton, and L. M. Jones (1990). The San Andreas fault system, California: seismicity 1980–1986, *U.S. Geol. Surv. Profess. Pap. 1515,* 115–152.

Holbrook, W. S., T. M. Brocher, U. S. ten Brink, and J. A. Hole (1996). Crustal structure beneath the San Francisco Bay block and the central California margin, *J. Geophys. Res.* **101,** 22311–22334.

Hole, J. H. and B. C. Zelt (1995). 3-D finite-difference reflection travel times, *Geophys. J. Int.* **121,** 427–434.

Hole, J. A., H. Thybo, and S. L. Klemperer (1996). Seismic reflections from the near-vertical San Andreas Fault, *Geophys. Res. Lett.* **23,** 237–240.

Jones, D. L., R. Graymer, C. Wang, T. V. McEvilly, and A. Lomax (1994). Neogene transpressive evolution of the California Coast Ranges, *Tectonics* **13,** 561–574.

Kelson, K. I., W. R. Lettis, and M. Lisowski (1992). Distribution of geologic slip and creep along faults in the San Francisco Bay region, in *Proc. on the Second Conference on Earthquake Hazards in the Eastern San Francisco Bay Area,* G. Borchardt (Editor), *Calif. Div. Mines Geol. Spec. Publ. 113,* 31–38.

Kern, H. and H. Wenk (1990). Fabric related velocity anisotropy and shear wave splitting in rocks from the Santa Rosa mylonite zone, California, *J. Geophys. Res.* **95,** 11213–11223.

King, N. E., P. Segall, and W. H. Prescott (1987). Geodetic measurements near Parkfield California, 1954–1984, *J. Geophys. Res.* **92,** 2747–2766.

Lisowski, M., J. C. Savage, and W. H. Prescott (1991). The velocity field along the San Andreas fault in central and southern California, *J. Geophys. Res.* **96,** 8369–8389.

Luetgert, J. H. (1992). MacRay-Interactive two-dimensional seismic raytracing for the Macintosh, *U.S. Geol. Surv. Open-File Rept. 92-356.*

McCarthy, J. and P. Hart (1993). Data report for the 1991 Bay Area seismic imaging experiment (BASIX), *U.S. Geol. Surv. Open-File Rept. 93-0301.*

McLaughlin, R. J., W. V. Sliter, D. H. Sorg, P. C. Russell, and A. M. Sarna-Wojcicki (1996). Large-scale right-slip displacement on the east San Francisco Bay region fault system, California: implications for location of late Miocene to Pliocene Pacific plate boundary, *Tectonics* **15,** 1–18.

Olson, J. and G. A. Lindh (1985). Seismicity of the San Andreas Fault from Cienega Winery to the Golden Gate, in *Minutes of the National Earthquake Prediction Evaluation Council, July 26–27, 1985, Menlo Park, California,* C. F. Shearer (Editor), *U.S. Geol. Surv. Open-File Rept. 85-0754,* 316–324.

Olson, J. A. and M. L. Zoback (1992). Seismic deformation patterns on the San Francisco Peninsula, *EOS* **73,** 401.

Page, B. M. (1992). Tectonic setting of the San Francisco Bay Region, in *Proc. on the Second Conference on Earthquake Hazards in the Eastern San Francisco Bay Area,* G. Borchardt (Editor), *Calif. Div. Mines Geol. Spec. Publ. 113,* 1–7.

Page, B. M. and T. M. Brocher (1993). Thrusting of the central California margin over the edge of the Pacific plate during the transform regime, *Geology* **21,** 635–638.

Parsons, T. and M. L. Zoback (1997). Three dimensional upper crustal velocity structure beneath San Francisco Peninsula, California, *J. Geophys. Res.* **102,** 5473–5490.

Ross, D. C. (1978). The Salinian Block: a Mesozoic granite orphan in the California Coast Ranges, in *Mesozoic Paleogeography of the Western United States, Pacific Coast Paleogeography Symposium 2,* D. G. Howell and K. A. McDougall (Editors), Pacific Section, Society of Economic Paleontologists and Minerologists, Los Angeles, California, 509–522.

Sanders, C. O. (1990). Earthquake depths and the relation to strain accumulation and stress near strike-slip faults in southern California, *J. Geophys. Res.* **95,** 4751–4762.

Siegesmund, S., M. Fritzsche, and G. Braun (1991). Reflectivity caused by texture-induced anisotropy in mylonites, in *Continental Lithosphere: Deep Seismic Reflections,* R. Meissner *et al.* (Editors), *Geodynamics Series 22,* American Geophysical Union, 21–29.

Stein, R. S. and M. Lisowski (1983). The 1979 Homestead Valley earthquake sequence, California: control of aftershocks and postseismic deformation, *J. Geophys. Res.* **88,** 6477–6490.

Taylor, C. L., J. C. Cummings, and A. P. Ridley (1980). Discontinuous en echelon faulting and ground warping, Portola Valley, California, in *Studies of the San Andreas Fault Zone in Northern California,* R. Streitz and R. W. Sherburne (Editors), *Spec. Rept. Calif. Div. Mines Geol.* **140,** 59–70.

Thatcher, W. (1975). Strain accumulation and release mechanism of the 1906 San Francisco earthquake, *J. Geophys. Res.* **80,** 4862–4872.

Thurber, C. H., S. Roecker, W. Lutter, and W. Ellsworth (1996). Imaging the San Andreas fault with explosion and earthquake sources, *EOS* **77,** 45–58.

Vidale, J. E. (1988). Finite-difference calculation of traveltimes, *Bull. Seism. Soc. Am.* **78,** 2062–2076.

Vidale, J. E. (1990). Finite-difference calculation of traveltimes in three dimensions, *Geophysics* **55,** 521–526.

Wallace, T. C., A. Velasco, J. Zhang, and T. Lay (1991). A broadband seismological investigation of the 1989 Loma Prieta California earthquake: evidence for deep slow slip? *Bull. Seism. Soc. Am.* **81,** 1622–1646.

Wang, C., D. A. Okaya, C. Ruppert, G. A. Davis, T. Guo, Z. Zhong, and H. Wenk (1989). Seismic reflectivity of the Whipple Mountain shear zone in southern California, *J. Geophys. Res.* **94,** 2989–3005.

Warner, M. (1990). Absolute reflection coefficients from deep seismic reflections, *Tectonophysics* **173,** 15–23.

Waters, K. H. (1987). *Reflection Seismology,* Wiley, New York, 538 pp.

U.S. Geological Survey
MS 999
Menlo Park, California 94025
E-mail: tparsons@usgs.gov

Manuscript received 4 November 1997.